Sensors & Diagnostics

PAPER

View Article Online
View Journal | View Issue

Cite this: *Sens. Diagn.*, 2024, **3**, 1866

Modulation of the binding sites for an adaptable DNA interactive probe: efficient chromo-fluorogenic recognition of Al^{3+} and live cell bioimaging†

Atanu Maji, Debarpan Mitra, Amitav Biswas, Moumita Ghosh, Rahul Naskar, Saswati Gharami Nabendu Murmu and Tapan K. Mondal *

Herein, a chromone-based simple reversible fluorescent "turn-on" probe, HMCP [6-(hydroxymethyl)-*N*′-((6-methyl-4-oxo-4*H*-chromen-3-yl)methylene)picolinohydrazide], was successfully utilized to detect Al^{3+} over a group of other coexisting metal cations in MeOH/H_2O (9 : 1, v/v) (HEPES buffer, pH = 7.2). The "turn on" emission response along with the effective enhancement of the fluorescence intensity upon addition of Al^{3+} can be attributed to the inhibition of photo-induced electron transfer (PET) and C=N isomerization, as well as the initiation of chelation-enhanced-fluorescence (CHEF). The HMCP sensor binds Al^{3+} in a 1 : 1 stoichiometry with an excellent binding constant and good detection limit on the orders of 10^3 M^{-1} and 10^{-7} M, respectively. The mode of binding interaction between HMCP with Al^{3+} was evidenced by ^1H NMR titration, HRMS, and Job's plot analyses. Theoretical calculations and molecular logic gate applications were also used to demonstrate the binding mode. A DNA binding study was also executed to elucidate the possible bioactivity of the probe and found that HMCP interacts with DNA more effectively than the other analogues studied. Furthermore, the applicability of the probe in a live cell imaging study indicated that HMCP is highly efficient for the detection of exogenous Al^{3+} in living cells. In addition, real water sample analysis and a dip-stick experiment demonstrate that the probe can be used in a wide range of practical and convenient applications.

Received 30th June 2024,
Accepted 10th September 2024

DOI: 10.1039/d4sd00242c

rsc.li/sensors

Introduction

Materials comprising of multiple applications are important and an emerging field in modern science. A Schiff base is one such kind of material. The low cost, user-friendliness and speed of use of Schiff bases has led to attempts to use them for sustainable development in pharmacy, medicine, molecular memory storage, chemical synthesis and analysis, photochromic materials and in colorimetric and fluorometric chemosensors.[1–6] Several analytical scientific techniques have been developed for the recognition of metal ions including spectrometry, chromatography, spectrophotometry, titrimetry and electrochemical strategies.[7,8] The above mentioned methods are complicated, lengthy and costly. Of the various techniques utilized for metal ion recognition, fluorescence signaling is one of the first preferences as it is reliable, simple, rapid as well as profoundly sensitive for the recognition of environmentally and biologically important metal ions.[9,10]

Aluminum is the third most abundant metal of all elements (after oxygen and silicon) and the most plentiful (8.3% by weight) metallic element in the Earth's crust. The extensive use of aluminum in our daily life appears in diverse areas, for example, in cosmetics, food packaging, medicine, water purification systems, food additives and electronic devices. Thus, the probability of human exposure to aluminum has increased, leading to a serious concern in recent years.[11] In addition, the concentration of Al^{3+} in soil and water resources has dramatically increased due to acid rain and thus inhibits the growth of plant and aquatic ecosystems.[12–20] As directed by the WHO (World Health Organization), the weekly permissible intake limit of Al^{3+} by human beings is around 7 mg kg^{-1} of body weight.[21] On the other hand, long-term intake of excess Al^{3+} could cause major diseases, for example, Alzheimer's, Parkinson's, kidney stones, osteoporosis, cardiac arrest, anemia, headaches, rickets, dementia and many more.[22–27] Doctors refers to Al^{3+}

Department of Chemistry, Jadavpur University, Kolkata-700032, India.
E-mail: tapank.mondal@jadavpuruniversity.in

† Electronic supplementary information (ESI) available: NMR and MS spectra of all new compounds, limit of detection determination, quantum yield calculations, CCDC no. 1535847 & 1535849 *etc.* See DOI: **https://doi.org/10.1039/d4sd00242c**

as the "silent killer" in human body because of possible connection to the brain.[28] Therefore, because of the negative impact of the excessive presence of Al^{3+} in the human body and environment, it is of great importance to develop some noteworthy tools with excellent properties in order to specifically recognise Al^{3+}, and to therefore regulate its environmental effects. DNA is one of the most important biomacromolecules in living beings that records hereditary traits. It controls the biosynthesis of various enzymes and proteins *via* replication and transcription. Therefore, DNA is the prime intracellular target of most hazardous substances and drugs. In general, duplex DNA binds with small molecules through various noncovalent interactions.[29] Due to the non-fluorescent nature of DNA, the main physiochemical experiments to investigate the interaction of small molecules with DNA are absorption and emission spectroscopy. A better understanding of the interactions of small molecules with DNA are in great demand in recent times and further encourage the pursuit of applications such as DNA molecular probes as well as chemotherapeutic reagents.[30–32]

The construction of semiconductors based on molecular logic gate functions is of specific interest, and they are extensively used in modern computing, in which the relationship between the input and output might be demonstrated by a truth table, where "1" denotes an active input/output and "0" as inactive one. Since, de Silva *et al.* developed the molecular AND logic circuit for the first time,[33] many research groups have utilized molecular logic gates in different applications.[34,35] For applications in data storage, many molecular logic gates have been constructed based on the specific recognition and detection of cations and anion.[36]

To date, many research groups have reported fluorescent sensors based on different fluorophore units for the specific recognition of Al^{3+}. For example, S. L. Hu *et al.* developed a simple pyrazoline-based fluorescent probe for Al^{3+} in aqueous solution that exhibited fluorescence quenching.[37] Zhang *et al.* developed a highly sensitive naphthalimide-based sensor (NPP) which detects Al^{3+} with a significant enhancement in fluorescence intensity and a detection limit that is determined to be 39 nM. Meanwhile, Wang *et al.* fabricated a tetrastyrene based fluorescence probe (L) showing a low detection limit of 1.587×10^{-7} M for Al^{3+} in a methanol–water (9/1, v/v) mixed solvent. Both probes show strong fluorescence emission in living cells.[38,39] Recently, Hwang *et al.* reported a simple Schiff base probe for live cell imaging studies which selectively binds with aluminum with a very low detection limit of 290 nM.[40] In 2022, Das *et al.* reported a chromone-based fluorescent switch for multi-analyte detection which displayed a prominent "turn-on" fluorescence response for Al^{3+} (LOD = 6.9 μM) in an aqueous medium.[41] Liu *et al.* synthesized a chromone derivative for the sole detection of Al^{3+} in EtOH with a detection limit of 0.214 μM.[42]

Considering the HSAB (hard and soft acids and bases) principle where the hard acid Al^{3+} always prefer to bind with the hard coordination sphere of donor atoms like "O" or "N" at suitable position to form stable chelate complex, we intend to introduce a very simple and low cost novel chromone-based probe, HMCP. The probe HMCP shows higher sensitivity over its analogues towards Al^{3+} in MeOH/H_2O (9 : 1, v/v) (HEPES buffer, pH = 7.2) based on PET and C=N isomerization as well as the CHEF mechanism. Upon titration with EDTA, the probe, HMCP, shows a reversible nature due to the dissociation of the HMCP-Al^{3+} complex followed by formation of a stable complex Na[Al(EDTA)]. Experimental outcomes are well verified using theoretical calculations. The possible bioactivity of HMCP was also examined through DNA binding studies. Cell imaging using breast cancer cells as well as real sample analysis have also been carried out to display some extensive potential practical utilization of the probe (HMCP).

Results and discussion

Synthesis of HMCP and its analogues

The synthetic path towards HMCP and its analogues (MCMP and MCMB) are depicted in Scheme 1. 6-(Hydroxymethyl) picolinohydrazide, picolinohydrazide and benzohydrazide were synthesized using reported literature procedures.[43–46] Reflux condensation of 6-methyl-4-oxo-4*H*-chromene-3-carbaldehyde and 6-(hydroxymethyl)picolinohydrazide in ethanol for 4 h affords the desired compound HMCP with a high yield (86%). In the same way, the analogues MCMP and MCMB were fabricated through the reflux condensation of 6-methyl-4-oxo-4*H*-chromene-3-carbaldehyde with picolinohydrazide and 6-methyl-4-oxo-4*H*-chromene-3-carbaldehyde with benzohydrazide in ethanol for 3 h with yields of 83% and 85%, respectively. The chemical structures of HMCP, MCMP and MCMB were confirmed using ^{1}H NMR, ^{13}C NMR and ESI mass spectrometry (Fig. S1–S9†).

Sensing studies of HMCP and its analogues using UV-vis spectroscopy

In order to investigate the interaction of HMCP with Al^{3+} in depth, UV-visible and emission studies were carried out in MeOH/H_2O (9 : 1, v/v) at 25 °C at physiological pH (10 mM HEPES buffer, pH = 7.2). The sensor HMCP displays a

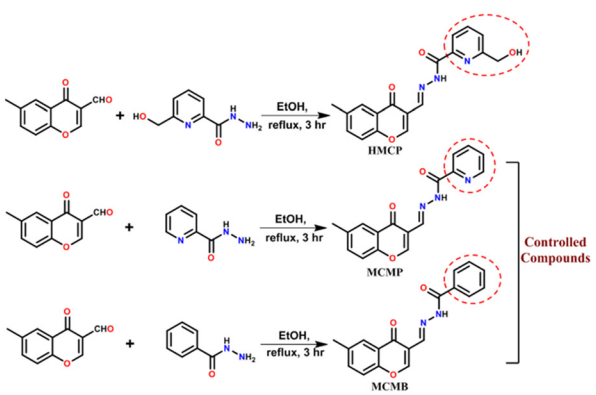

Scheme 1 Synthetic scheme of the synthesis of the investigated probe, HMCP, and its analogues (MCMP & MCMB).

moderate absorbance band at 315 nm along with a shoulder peak at 283 nm. Upon incremental addition of Al^{3+} into the solution of HMCP, the intensity of the former absorbance peaks at 315 nm and 283 nm were gradually decreased and the simultaneous emergence of a new absorption band at 424 nm along with two closely situated bands at 408 nm and 448 nm were noticed with the formation of a distinct isosbestic point at 351 nm (Fig. 1). The appearance of new absorption bands at 424 nm along with two small shoulders at 408 nm and 448 nm and the distinct color change is supporting evidence of the complexation of Al^{3+} to HMCP. To establish the selectivity of the probe (HMCP), the UV-visible spectra of HMCP were recorded in presence of other metal cations such as Na^{+}, Mg^{2+}, Mn^{2+}, Ba^{2+}, Bi^{3+}, La^{3+}, Ce^{3+}, Ga^{3+}, In^{3+}, Fe^{3+}, Cr^{3+}, Co^{2+}, Ni^{2+}, Hg^{2+}, Zn^{2+}, Cu^{2+}, Pb^{2+} and Cd^{2+}. No significant absorbance change was observed in the presence of any of the other metal cations, except only for Zn^{2+} and Cu^{2+} (Fig. 1). The absorption spectra of MCMP and MCMB were also studied. The probe MCMP itself shows a strong absorption band at 313 nm along with a small shoulder at 281 nm. In presence of Al^{3+}, the absorption intensity at 313 nm and 281 nm gradually decreases followed by the appearance of a new absorption band at 422 nm with two closely situated small humps (Fig. S10†). Similarly, upon addition of Al^{3+} into the probe solution of MCMB, the absorption band at 310 nm for the free probe MCMB gradually decreases along with the appearance of a new band at 412 nm with a small hump at 398 nm. These outputs confirm the coordination of Al^{3+} to the analogues (MCMP and MCMB). Two distinct isosbestic points at 347 nm and 354 nm were also noticed for MCMP and MCMB, respectively. In the presence of other metal ions, the absorption spectra of both the analogues were recorded and it was noted that none of the abovementioned metal ions caused any noteworthy changes in the emission profile of the analogues, except Zn^{2+} and Cu^{2+}. Therefore, HMCP and its analogues (MCMP and MCMB) are highly selective towards Al^{3+}.

Sensing studies of HMCP and its analogues using emission spectroscopy

The fluorescence spectral pattern revealed that upon excitation at 351 nm, the HMCP probe displays a broad centered emission band at 471 nm with very low intensity. This very low fluorescence intensity can be ascribed to the combined effects of PET and C=N isomerization *via* non-radiative decay processes from the excited state. The sequential addition of Al^{3+} into the probe solution resulted in a significant enhancement in the fluorescence intensity (~14 fold) at around 496 nm with an increase in the quantum yield (φ) from 0.03 to 0.21 (Fig. 2). The "turn-on" emission response of HMCP towards Al^{3+} could be explained on the basis of the strong binding affinity of Al^{3+} with HMCP, which prohibited both the C=N isomerization and PET processes in the receptor, thereby initiating increasing rigidity in the complex resulting in chelation enhanced fluorescence (CHEF). The change in the fluorescence properties of HMCP was examined in the presence of other coexisting metal ions, but there is hardly any change in the fluorescence intensity of HMCP (Fig. 2). Therefore, the receptor, HMCP is highly efficient at detecting Al^{3+} fluorimetrically with a significant emission enhancement followed by a prominent fluorescence color change from colorless to intense cyan. This fluorescence enhancement falls under the category of strong "OFF–ON" fluorescence properties. Further, on sequential addition of EDTA to the solution of HMCP-Al^{3+}, the fluorescence intensities at 484 nm as well as at 466 nm reverted back to the original emission intensity of the probe (HMCP) itself which clearly establishes the fact that HMCP has returned to its free state (Fig. 3) thereby making the sensor a reversible fluorescent switch. Hence, HMCP can serve as an "OFF–ON–OFF" fluorescence signaling sensor.

From the fluorescence spectral changes, the detection limit of HMCP for Al^{3+} was determined using the equation, LOD = $K \times SD/S$, where "SD" is the standard deviation of the blank solution of the probe and "S" in the slope of the curve. Thus, the LOD was found to be $(3.12 \pm 0.12) \times 10^{-7}$ (M) (Fig. S13†). This low detection limit evidently demonstrates the fact that HMCP is highly efficient in detecting Al^{3+} at very minute concentrations. The association constant (K_a) of HMCP for Al^{3+} was also calculated using the Benesi–Hildebrand equation and found to be $(9.34 \pm 0.45) \times 10^{3}$ M^{-1} (Fig. S14†), which signifies that the HMCP-Al^{3+} complex is notably stable.

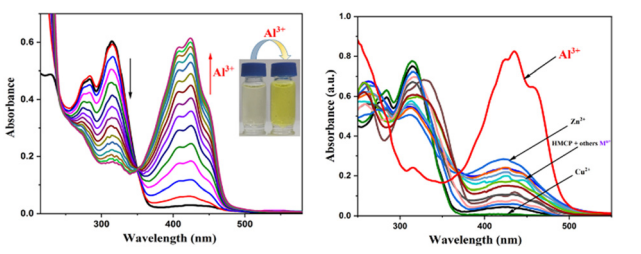

Fig. 1 Change in UV-vis spectrum of HMCP (10 μM) upon successive addition of Al^{3+} (0–20 μM) in MeOH (left side) and in the presence of different metal ions (40 μM) in MeOH/H_2O (9 : 1, v/v) (HEPES buffer, pH = 7.2) (right side).

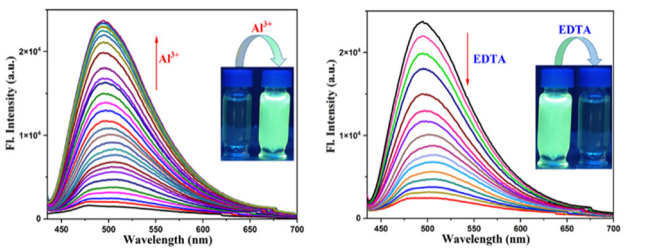

Fig. 2 Change in emission spectra of HMCP (10 μM) upon gradual addition of Al^{3+} (0–20 μM) in MeOH/H_2O (9 : 1, v/v) (HEPES buffer, pH = 7.2) (left side). Inset shows the change in colour under UV-radiation. Change in emission spectra of HMCP (10 μM) upon incremental addition of EDTA (0–20 μM) into HMCP : Al^{3+} complex solution (right side). Inset shows the change in colour under UV-radiation.

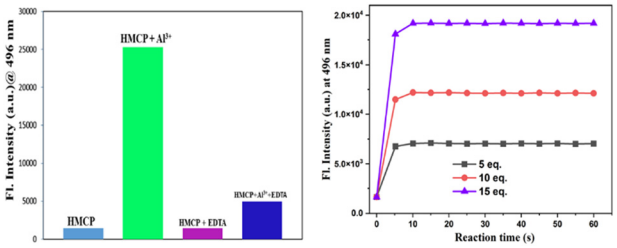

Fig. 3 Variation of the fluorescence intensity of HMCP in the presence of Al^{3+} and EDTA (left side). Time-dependent fluorescence response of HMCP (10 μM) to different concentrations of Al^{3+} ions (5–15 μM) in MeOH/H_2O (9 : 1, v/v) (HEPES buffer, pH = 7.2) solution at 496 nm.

To better comprehend the excited state stability of this fluorescent switch, the lifetimes of HMCP and HMCP-Al^{3+} were also measured. The fluorescence lifetime of the free probe (HMCP) shows a mono-exponential decay pattern and was found to be 1.12 ns while the HMCP-Al^{3+} complex exhibits a bi-exponential decay (measured at λ_{em} = 351 nm) with a lifetime value of 4.24 ns. The increase in lifetime is attributed to the decrease in non-radiative decay due to the structural rigidity of the complex relative to the comparatively more flexible free probe. On the other hand, after the addition of EDTA, the lifetime of HMCP-Al^{3+} again decreases and was found to be 1.53 ns, suggesting that the dissociation of the complex to the free HMCP had occurred (Fig. S15 and Table S4†).

In order to investigate the specificity of the probe towards Al^{3+}, the fluorescence intensity of the probe solution containing other metal cations was recorded separately before and after the addition of the Al^{3+} ions. It is observed from the competitive experiment that the fluorescence enhancement of HMCP upon addition of Al^{3+} is not significantly affected by the presence of other metal cations (Fig. S16†). Therefore, HMCP is highly specific towards Al^{3+}.

pH study

pH titration experiments were performed on HMCP using a fluorescence method and the titration indicated the fact that the newly developed fluorescent probe HMCP does not experience any major change in its fluorescence profile at 496 nm. This finding suggests that the sensor, HMCP, operates independently of the pH. Now, with the presence of Al^{3+} in the HMCP solution, the fluorescence intensity increased gradually with an increase in the pH value, achieving maximum intensity at pH 7.2. This reveals that the probe is compatible for sensing Al^{3+} at neutral pH (Fig. S20†). After pH 7.2 was reached, the emission intensity gradually decreased due to the deprotonation of the –OH group, causing the dissociation of the complex, which eventually results in rendering HMCP unable to sense Al^{3+}. Hence, the newly designed probe HMCP is highly capable of detecting Al^{3+} in the neutral pH range with an excellent efficacy.

Recyclability and reusability

An ideal chemosensor must have two essential properties, recyclability and reusability. To examine the reversibility, a solution of HMCP was prepared in MeOH/H_2O (9 : 1, v/v) (HEPES buffer, pH = 7.2). Fig. S14† reveals that upon the addition of Al^{3+} to the HMCP solution, a "turn on" emission was observed. Subsequently, the addition of EDTA solution into the HMCP-Al^{3+} complex solution gives a "turn off" emission as the complex is dissociated due to the formation of a stable Na[Al(EDTA)] complex, releasing a free receptor. This observation signifies that the sensing capability of HMCP is reversible. To further confirm the reversible nature, the experiment was performed using a MeOH solution of HMCP for a second time. Upon further addition of Al^{3+} ions, the solution again gives a "turn on" emission and the sequential addition of EDTA shows a "turn off" emission response. Thus, an increase in the emission intensity of the HMCP solution upon addition of Al^{3+} and a quenching in the fluorescence intensity of the HMCP-Al^{3+} complex in the presence of EDTA was observed over four cycles, with little loss in sensing efficacy (Fig. S17†). Such reversibility and regeneration are important for the design of devices to recognize Al^{3+} ions.

A chemosensor with a rapid fluorescence response is always highly preferable for practical purposes. Time-dependent experiments were executed in order to interpret the instant emission response of the HMCP sensor. At different time intervals, the emission intensity was monitored in the presence of different concentrations of Al^{3+} (5 μM, 10 μM, and 15 μM). Fig. 3 shows that our investigated probe HMCP is highly efficient at detecting Al^{3+} within a very short time span (0–10 seconds) after the addition of the Al^{3+} ions. 10 seconds after Al^{3+} addition, the emission intensity at 496 nm almost reached its saturation level, which signifies completion of the reaction. Hence HMCP can serve as a powerful and reliable sensor for the recognition of aluminum ions within a short time period (0–10 s).

Photosensitivity study

For fluorescence based sensing applications, a probe that has high photo-stability whilst exhibiting steady analytical signals is highly preferable. Therefore, in order to evaluate the photosensitivity of the newly designed sensor, HMCP and the HMCP-Al^{3+} complex were irradiated over 2 min in day light under optimal conditions according to the previously reported literature.[47,48] Fig. S22† indicates that the sensor HMCP and complex HMCP-Al^{3+} had high photostability throughout the experiment (2 min) with negligible changes in emission intensity. Therefore, these experimental results suggest that HMCP has a highly photostable "turn-on" fluorescence signal response in the presence of Al^{3+}, making it highly competent for the spectrofluorimetric analysis of real samples.

Probable sensing mechanism of HMCP

The enhancement in the emission intensity of HMCP and its analogues in the presence of Al^{3+} is possibly accredited to the combined effect of two important mechanisms, PET and C=N

isomerization (Fig. 5). These mechanisms are on in the free probes, but after binding with Al^{3+}, these two mechanisms were inhibited and rigidity in the complex is induced, thus accounting for the enhancement in fluorescence intensity. In addition, due to the presence of several oxygen and nitrogen donor centres, it was anticipated that the probe and its analogues have strong affinity for chelation with the hard acid Al^{3+}, according to the HSAB principle.

The nature of the binding mode of the chemosensor HMCP towards Al^{3+} was investigated *via* a ^{1}H NMR titration study. The signal at δ = 12.98 ppm can be assigned to the proton (H_b) of the –NH–C═O unit (Fig. 4). Upon interaction with the Al^{3+} ions, the H_b proton of the amide unit gradually shortens and meanwhile a new peak is noticed at 9.23 ppm due to the conversion of the amide into an imidic acid tautomer (–(N═C(OH))–).[45] Furthermore, the imine proton (H_a) peak at 6.78 ppm underwent a slight down-field shift, thereby confirming the participation of the imine nitrogen atom in complex formation. The HRMS spectrum of HMCP exhibits a peak at *m*/*z* 360.0491, possibly due to the [HMCP + Na]$^+$ ion, whereas the HMCP-Al^{3+} complex exhibits a peak at *m*/*z* 542.0648 indicating the formation of a mononuclear complex between HMCP and Al^{3+} (Fig. S21†). The binding stoichiometry of HMCP to Al^{3+} (1 : 1) was further supported by a Job's plot analysis (Fig. S18†). Therefore, the ^{1}H NMR, HRMS, and Job's plot analyses gave strong evidence for the proposed binding mode depicted in Fig. 6.

The cyan fluorescence response of MCMB in the presence of Al^{3+} established the fact that the pyridinium nitrogen atoms of HMCP and MCMB do not participate in the complex formation and further supported the binding mechanism depicted in Fig. 6. The greater emission intensity enhancement observed for HMCP and MCMP compared to MCMB upon addition of Al^{3+} can be attributed to the –I effect

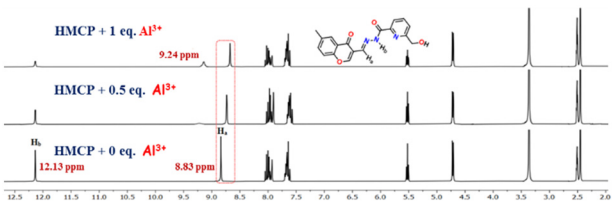

Fig. 4 ^{1}H NMR titration experiments to elucidate the sensing mechanism of HMCP upon addition of different concentrations of Al^{3+}.

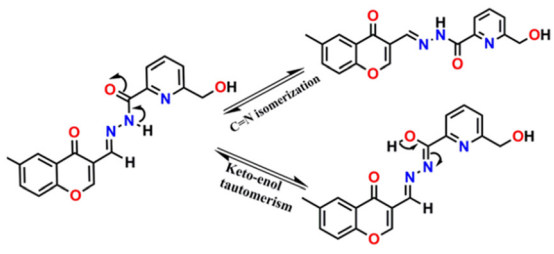

Fig. 5 Keto-enol tautomerism and C═N isomerization processes in the HMCP probe.

Fig. 6 Probable sensing mechanism of HMCP with Al^{3+}.

of the pyridine moiety which favours the formation of the enol form of both HMCP and MCMP (Table S1†). Again, the large emission intensity enhancement of HMCP compared to MCMP in presence of Al^{3+} is due to the presence of the additional aliphatic hydroxyl group (–CH_2OH) which increases the solubility of HMCP through H-bonding, thereby displaying a higher emission intensity.

DNA binding study

The binding of DNA with sensors is in high demand for the design and development of new targeted drugs. Ligands can bind with DNA through various non-covalent interactions. The affinity of HMCP and its analogues toward ct-DNA were examined through the changes in absorption and emission spectra (Fig. 7). Generally, a change in the absorption spectra, whereby a new peak appears at a new location, is observed when a complex is formed by the interaction of a small molecule/ligand with ct-DNA. The absorption spectra of HMCP was recorded upon addition of ct-DNA. Fig. 7 reveals the fact that upon incremental addition of ct-DNA into the HMCP probe solution, the inherent absorption band of HMCP at 315 nm gradually diminishes along with the appearance of two new absorption bands at 356 nm and 266 nm. Here, ct-DNA absorption is insignificant, suggesting the existence of an effective interaction between the π electron cloud of the interfacing sensor HMCP and the base pairs of DNA along with H-bonding.[49]

Upon excitation at 331 nm, the HMCP sensor displays an emission band at 471 nm. After successive addition of ct-DNA into the HMCP solution, about an 8-fold enhancement in the fluorescence intensity was detected at 476 nm (Fig. 7).

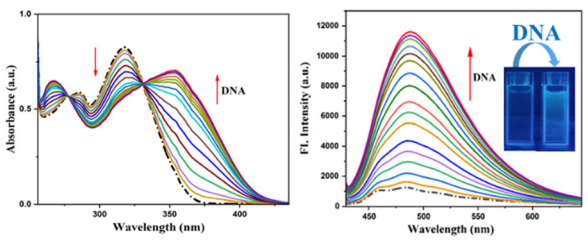

Fig. 7 Change in UV-vis spectrum of HMCP (10 μM) upon addition of ct-DNA (0–20 μM) in MeOH (left side) and change in emission spectra of HMCP (10 μM) upon addition of ct-DNA (0–20 μM) in MeOH (right side).

This significant rise in fluorescence intensity with a distinct fluorescence color change upon association with ct-DNA implies that an effective non-covalent interaction exists between the HMCP sensor and the DNA. The magnitude of the apparent equilibrium constant K_{BH} between HMCP and ct-DNA was assessed spectrofluorimetrically (Benesi–Hildebrand plot) and was found to be 2.66×10^4 M^{-1} (Fig. S23†). The turn on fluorescence response can be attributed to the PET process, which is interrupted upon binding with DNA and may be due to the interaction of the lone pair of the HMCP imine nitrogen with the π-electron clouds of the DNA (Fig. 8). The "turn-on" emission enhancement of MCMP and MCMB upon addition of ct-DNA was also recorded and the outcomes are summarized in Table S2.† The higher enhancement in the fluorescence intensity for HMCP compared to MCMP may be due to the presence of an aliphatic –OH group in HMCP which initiates additional H-bonding interactions followed by stronger binding with DNA compared to that of MCMP. Again, the higher emission intensity of MCMP compared to MCMB may be because the presence of the additional lone pair of electrons on the pyridinium nitrogen atom allows for a more extensive interaction with the DNA base pairs as compared to MCMB.

Molecular logic gate

The emission properties of the HMCP sensor compelled us to investigate its application in numerous logic gates by successive addition of inputs, like metal cations such as Al^{3+} and anionic species like EDTA, whilst recording its fluorescence at 496 nm as the output. Inputs are denoted as "1" for their presence and their absence are assumed to be "0". Outputs are denoted as "1" when the fluorescence intensity is above a certain threshold value (25% of the maximum). When no input is present, no characteristic fluorescence is noted and is considered to be "0" (off state). From the truth table, it is observed that HMCP shows an emission intensity output signal with Al^{3+} (input A) in such a manner that it seems to realise the requirements of an "AND" operation. In the presence of EDTA (input B), HMCP realizes a "NOT" operation (Fig. 9). Furthermore, when both inputs (Al^{3+} and EDTA) are present, the output emission intensity decreases, indicating the off state according to the truth table. These data are related to an "INHIBIT" logic gate *via* a particular arrangement of the logical functions AND and NOT.

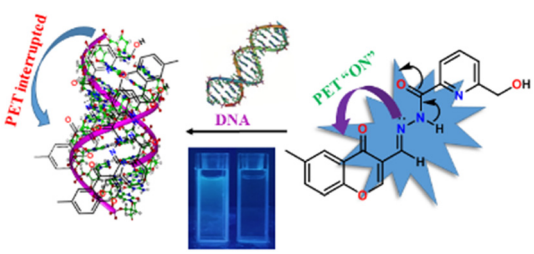

Fig. 8 Interaction between the interfacing ligand and ct-DNA.

Entry	Input A (Al^{3+})	Input B (EDTA)	Output Emission@ 496 nm
1	0	0	0
2	1	0	1
3	0	1	0
4	1	1	0

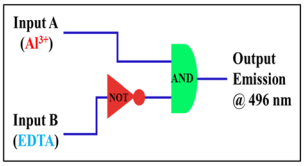

Fig. 9 Truth table for advance-level molecular logic gate (left side) and corresponding circuit diagram (right side).

Molecular memory device

The techniques for data storing are well known and can be combined by successive logic circuits. The combination of these circuits creates the following response loop where one of the output signals is assumed to be the input of the memory device and is considered as the "memory element". The function of the memory device is built on a binary logic; either 1 or 0 alternates the two crisp states. In our device, for establishing a suitable mimic of the memory component, we consider Al^{3+} and EDTA as the set (S) and reset (R) inputs respectively and the fluorescence intensity at 496 nm as the output signal. In the memory device function, input A (Al^{3+}) is considered as the set (S) and binary state 1 appears. However, the written data is erased under the reset input (EDTA) and binary state "0" is recorded. So, by applying a binary logic function, we have successfully established a consecutive logic circuit displaying a "write–read–erase–read" feature (Fig. 10). It is worth mentioning that the write–erase cycles could be reversed repeatedly several times with the same complex solution without a significant decrease in the fluorescence intensity. Thus, the circuits developed in this manner function comparably to logic memory devices of conventional semiconductors and can be considered as a better technique that can be possibly explored in the near future for the setup of molecular microprocessors of integrated circuits.

Practical application as a dip-stick: detection of Al^{3+} using a TLC plate

For the qualitative identification of Al^{3+}, we have carried out an experiment known as a dip-stick experiment where the sensor can act as a portable fluorescence kit, also exhibiting its sensing capability towards the specific metal ion in the solid state without the aid of any sophisticated instruments. In order to execute this experiment, a few thin-layer

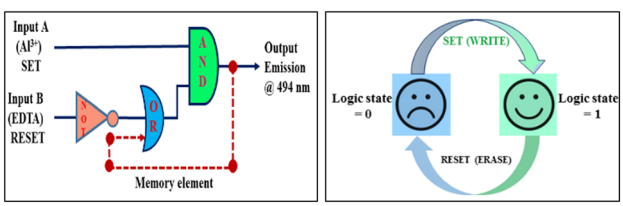

Fig. 10 Consecutive logic gate of a memory unit (left side) and schematic representation of the reversible logic operation of the memory element with a write–read–erase–read function (right side).

chromatography (TLC) plates were prepared and they were immersed into a solution of HMCP (2×10^{-4} M) in MeOH and then dried by evaporating the solvent. Next, the dried probe-coated TLC plates were immersed into an Al^{3+} solution (2×10^{-3} M) and then the solvent was evaporated again in order to dry the plates. The visual colour change of the probe-loaded TLC plates in the absence and presence of Al^{3+} was prominent and distinguishable in day light as well as under UV light (Fig. 11). This method helps one to thoroughly and easily identify the presence of Al^{3+} using the naked eye.

Real sample analysis

In order to validate the practical utility of our approach, the feasibility of the probe was investigated for the detection of aluminium ions in different water samples (tap and lake water) *via* fluorescence method according to previously reported methods.[50,51] The samples were first filtered and then used for further experiment. These natural water samples were not subjected to the detection method. Now various concentrations of Al^{3+} ion were mixed into these natural water samples and the HMCP probe was successfully employed for the determination of aluminium content in these real water samples. From the experimental outcomes summarized in Table S3,† it is concluded that the HMCP sensor is highly proficient at detecting the concentration of Al^{3+} in contaminated natural water samples with excellent recovery rates (96.5–100.2%).

Application in the biological field of live cell imaging in human breast cancer cells

From the MTT experiments, it can be concluded that the receptor, HMCP, has negligible toxicity towards human breast cancer cells (MDA-MB-231) at lower concentrations (Fig. 12). The IC_{50} value of HMCP was determined and found to be 189.6 μM and therefore we have preferred the dose, when conducting this experiment, to be 15 μM as the chosen dose should be less than the IC_{50} value (Fig. S19†). Now, the fluorescence imaging experiment under the microscope revealed that the treatment of the breast cancer cells with HMCP itself exhibits no fluorescence, but following incubation of the MDA-MB-231 cells with 15 μM of aluminum and HMCP, a bright blue emission in the intracellular region was noticed (Fig. 12). This experiment established the fact that the HMCP sensor can easily penetrate the cell membrane in order to bind with the intracellular aluminum ion. Further, there is no physical change observed for the studied cells in bright field images after incubation with Al^{3+}, implying that the MDA-MB-231 cells are viable and HMCP is not toxic at that specific concentration (Fig. 12). Therefore, our present probe has a chance to serve as a cell membrane-penetrable fluorescence kit that has excellent biological applications in living cells for analyzing exogenous Al^{3+} ion content.

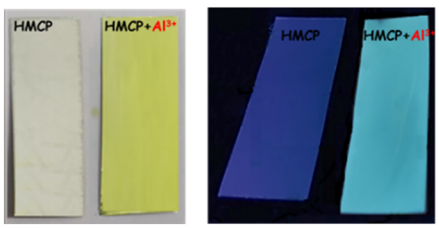

Fig. 11 Pictures of TLC plates immersed in MeOH solution before and after being dipped into an Al^{3+} solution in normal light (left side) and in a UV chamber (right side). [HMCP] = 2×10^{-4} M, [Al^{3+}] = 2×10^{-3} M.

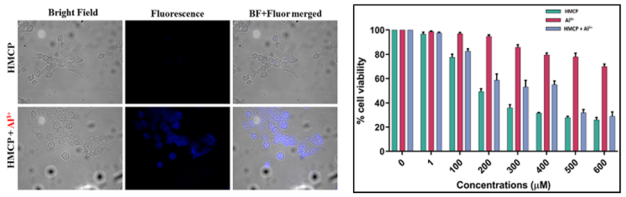

Fig. 12 (Left side) Fluorescence image of breast cancer cells after incubation with 15 μM HMCP and HMCP-Al^{3+} complex. DAPI is used to stain the nucleus. (Right side) MTT assay of HMCP, Al^{3+} and HMCP-Al^{3+} complex on human breast cancer cell lines.

Theoretical calculations

In order to understand the structural changes of HMCP upon binding with Al^{3+}, DFT calculations were executed using the B3LYP/6-31+G(d) method of the Gaussian 09 program. Fig. S24 and S25† represent the optimized structures of HMCP and its complex. Fig. S26 and S27† display the contour plots of some selected molecular orbitals (HOMOs) of HMCP and the HMCP-Al^{3+} complex, respectively. The HOMO–LUMO energy gap of HMCP is 4.13 eV, while for the HMCP-Al^{3+} complex, the HOMO–LUMO energy gap is decreased to 3.31 eV (Fig. 13). This effective change in the HOMO–LUMO energy gap is well supported by the bathochromic shift observed in the absorption spectrum upon addition of Al^{3+} into the probe solution. To interpret the electronic spectra, vertical electronic transitions were determined using time-dependent density-functional theory (TDDFT) calculations (solvent correction was incorporated by the CPCM model and

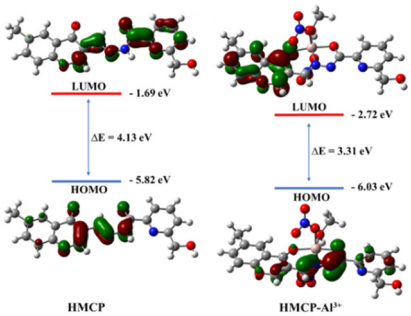

Fig. 13 HOMO–LUMO energy gap of HMCP before and after addition of Al^{3+}.

MeOH was chosen as the solvent) and are summarized in Table S6.† The calculated vertical excitations of HMCP show strong transitions at 335 nm (f = 0.7610) due to the HOMO → LUMO transition. However for HMCP-Al^{3+}, the HOMO → LUMO transition shifted to 380 nm (f = 0.0868) (Table S6†).

Conclusion

In conclusion, we have designed and successfully fabricated a chromone based OFF–ON–OFF reversible chemosensor HMCP, which is more efficient for detecting Al^{3+} than its analogues. The affinity of HMCP towards Al^{3+} rather than a group of other coexisting metal ions was accredited to the HSAB principle, where the hard centred N and O atoms in the probe prefer to bind with the hard acid Al^{3+} ions. The detection limit was determined based on fluorescence changes and found to be $3.12 \pm 0.12 \times 10^{-7}$ M. The "turn-on" chromo-fluorogenic response after binding with Al^{3+} was due to the restriction of C=N rotation and the inhibition of a PET process along with the initiation of chelation-enhanced-fluorescence (CHEF). The proposed binding mode of HMCP to Al^{3+} was supported by ^{1}H NMR titration, HRMS, and Job's plot analyses as well as DFT calculations. DNA binding studies were also performed to demonstrate the higher bioactivity of HMCP compared to its analogues. In addition, the synthesized HMCP probe was utilised in the selective detection of Al^{3+} in real water samples. Moreover, cellular imaging studies were also conducted to establish the Al^{3+} bio-sensing ability of HMCP in living cells (MDA-MB-231).

Experimental section

Materials and instrumentation

All the reagents and organic compounds used in this synthesis were purchased from Sigma-Aldrich. All the other solvents and inorganic salts used in the synthetic procedures were purchased from available commercial sources. DMSO-d_6 and $CDCl_3$ were used as the solvents for the NMR experiments without further distillation. Thin layer chromatography (TLC) was carried out using Merck 60 F_{254} plates with a thickness of 0.25 mm. A PerkinElmer Lambda 750 spectrophotometer was used to obtain the absorbance spectra and the emission properties were measured using a Shimadzu RF-6000 fluorescence spectrophotometer at room temperature (298 K). Lifetimes were measured using a time-resolved spectrofluorometer from IBH, UK.

Synthesis of 6-(hydroxymethyl)-*N*′-((6-methyl-4-oxo-4*H*-chromen-3-yl)methylene)picolinohydrazide (HMCP)

6-(Hydroxymethyl)picolinohydrazide (0.167 g, 1 mmol) was added to an ethanolic solution of 6-methyl-4-oxo-4*H*-chromene-3-carbaldehyde (0.19 g, 1 mmol) and the mixture was then refluxed for about 7 hours. After completion of the reaction, a white precipitate was obtained which was purified *via* column chromatography to yield the desired product (HMCP). The yield was 0.29 g, 86%.

^{1}H NMR data (300 MHz, DMSO-d_6). δ (ppm): 2.45 (s, 3H), 4.72 (d, J = 5.88 Hz, 2H), 5.52 (t, J = 6 Hz, 1H), 7.61–7.69 (m, 3H), 7.92–8.05 (m, 3H), 8.83 (s, 1H), 12.13 (s, 1H).

^{13}C NMR (75 MHz, DMSO-d_6). δ(ppm): 22.1, 50.21, 103.9, 110.4, 112.1, 116.7, 121, 123.6, 126.8, 127, 131, 132.6, 140, 144.7, 147.9, 148.8.

HRMS. Calculated for $C_{18}H_{15}N_3NaO_4$ $[M + Na]^+$ (m/z) = 360.0690; found = 360.0491.

Synthesis of (*E*)-*N*′-((6-methyl-4-oxo-4*H*-chromen-3-yl)methylene)picolinohydrazide (MCMP)

Picolinohydrazide (0.14 g, 1 mmol) was added to an ethanolic solution of 6-methyl-4-oxo-4*H*-chromene-3-carbaldehyde (0.19 g, 1 mmol) and the reaction mixture was refluxed for about 8 hours. After completion of the reaction, a white product appeared which was then subjected to column chromatography to get a pure white solid. The yield was 0.25 g, 83%.

^{1}H NMR data (300 MHz, DMSO-d_6). δ (ppm): 2.46 (s, 3H), 7.65 (s, 1H), 7.67–7.71 (m, 2H), 7.93 (d, J = 7.77 Hz, 1H), 8.03–8.14 (m, 2H), 8.80 (d, J = 6.87 Hz, 2H), 10.13 (s, 1H), 12.36 (s, 1H).

^{13}C NMR (75 MHz, DMSO-d_6). δ (ppm) 23.2, 51.2, 102.9, 103.9, 110.4, 112.1, 116.7, 121, 123.6, 126.8, 127, 131.8, 132.6, 140, 144.6, 146.8, 147.9.

HRMS. Calculated for $C_{17}H_{14}N_3O_3$ $[M + H]^+$ (m/z) = 308.1030; found = 308.0941.

Synthesis of (*E*)-*N*′-((6-methyl-4-oxo-4*H*-chromen-3-yl)methylene) benzohydrazide (MCMB)

An ethanolic mixture of benzohydrazide (0.14 g, 1 mmol) and 6-methyl-4-oxo-4*H*-chromene-3-carbaldehyde (0.19 g, 1 mmol) was refluxed carefully for about 7 hours. After completion of the reaction, a white precipitate was obtained which was subjected to column chromatography to yield the pure final product. The yield was 0.26 g, 85%.

^{1}H NMR data (300 MHz, DMSO-d_6). δ (ppm): 2.46 (s, 3H), 7.51–7.71 (m, 6H), 7.93 (d, J = 6.9 Hz, 2H), 8.64 (s, 1H), 8.82 (s, 1H), 11.94 (s, 1H).

^{13}C NMR (75 MHz, DMSO-d_6). δ (ppm) 21.3, 50.2, 102.9, 103.9, 110.2, 112.1, 113.7, 121, 123.6, 126.8, 127.4, 131.8, 132.5, 140, 144.7, 145.8, 147.9.

HRMS. Calculated for $C_{18}H_{15}N_2O_3$ $[M + H]^+$ (m/z) = 307.1077; found = 307.1206.

General method for UV-vis and fluorescence titration

UV-vis method. In order to record the UV-vis spectrum, a stock solution of the sensor, HMCP (10 μM), was prepared in MeOH/H_2O (9 : 1, v/v) (HEPES buffer, pH = 7.2) (at 25 °C). The solutions of all the competitive cations were prepared at concentration on the order of 1×10^{-5} M, in deionized water. Solutions of different concentrations of HMCP and all the metal cations were prepared separately. The UV-vis spectra of these sample solutions were monitored.

Fluorescence method. In order to record the fluorescence spectra, a stock solution of the probe, HMCP (10 μM), that was the same as that used for UV-vis method was prepared. The solutions of the guest metal ions, at concentrations on the order of 1×10^{-5} M, were prepared using deionised water. Different concentrations of the sample solutions containing the probe HMCP and metal ions were prepared separately. The spectra of these solutions were monitored by means of fluorescence technique.

Job's plot experiment. For this experiment, a series of sample solutions containing HMCP (10 μM) and Al^{3+} (20 μM) were prepared in such a way that the sum of the volume of the total metal cation and HMCP remained constant (4 mL) in MeOH/H_2O (9 : 1, v/v) (HEPES buffer, pH = 7.2). Job's plots were then plotted as a function of the emission intensity change at 496 nm *versus* the mole fraction of Al^{3+}.

Live cell imaging studies

Cell cytotoxicity assay. Human breast cancer cells (MDA-MB-231) were obtained from the National Centre for cell science, Pune, India and maintained in Eagle's minimum essential media (MEM) (Gibco, Life Technologies) and were supplemented with 10% fetal bovine serum (FBS) (Gibco, Life Technologies, USA) and stored at 37 °C in a humidified incubator under a 5% CO_2 atmosphere. The cytotoxicity of aluminium nitrate (Al^{3+}), HMCP and the HMCP-Al^{3+} complex towards the MDA-MB-231 cell lines was studied according to the procedure reported by Gharami *et al.*[52] The cells were seeded in 96-well plates at a density of 5×10^3 cells per well and cultivated in a CO_2 incubator for 22 h. Different doses (10, 25, 50, 75, 100, 125, 150, and 175 μM) of free HMCP, Al^{3+} and the HMCP-Al^{3+} complex were introduced into the cells separately along with a control for 24 h. Aluminum was dissolved in an aqueous medium while the sensor (HMCP) was dissolved in DMSO, although the final concentration of DMSO while treating the studied cells was maintained below 1%. After 24 h of treatment, a methyl tetrazolium dye (MTT) (5 mg mL^{-1}) solution was mixed into each well (10 μL per well). The well plates were then incubated in the dark at 37 °C for 2 h. To each well 100 μL of DMSO was mixed and allowed to settle for 1 h in a vortex shaker. Next, the cell viability efficiency was evaluated by recording the absorbance at 570 nm for each well using a microplate reader (Tecan, Infinite M200). The untreated cells were considered as 100% viable. The IC_{50} value of the free probe HMCP only was calculated by plotting a non-linear regression between the log of the concentration of HMCP and the O.D. value at 570 nm.

Cellular bio-imaging. Human breast cancer cells (MDA-MB-231) were grown overnight on 22 × 22 mm glass cover slips positioned at the bottom of six well plates. Then the cells were treated with 15 μM each of the probe, HMCP and the HMCP-Al^{3+} complex for 1 h. The IC_{50} value for HMCP was determined and found to be 189.6 μM. Based on the IC_{50} value, a dosage of 15 μM was selected. After treatment, the cells were then fixed with methanol and washed with 0.5% phosphate buffer saline tween (PBST) twice and then with 1 × PBS thrice. The cover slips then were mounted on a glass slide and were observed under a fluorescence microscope (Leica DM4000 B, Germany) at 20× magnification.

Computational methodology. Full geometry optimizations were performed using a density-functional theory (DFT) method at the B3LYP[53] level of theory for the ligand and complex. All calculations were carried out on the Gaussian 09 program package.[54] The calculations were aided by the Gauss View visualization program. All elements, except aluminium, were assigned to the 6-31+G(d)[55] basis set. The vibrational frequency calculations were executed to establish that the optimized geometries show the local minima and there were only positive eigen values. A time-dependent density-functional theory (TDDFT) formalism[56,57] was employed to compute the vertical electronic excitations based on the B3LYP optimized geometries in methanol using a conductor-like polarizable continuum model (CPCM).[58]

DNA-binding experiments

Absorption and fluorescence method. A stock solution of ct-DNA (10^{-3} M) was prepared using a buffer solution (pH = 7.2) and absorption and fluorescence titration were carried out upon gradual addition of ct-DNA. The addition of ct-DNA into the probe (HMCP) solution continued until saturation was achieved. These titration results are essential for the quantification of the equilibrium constant of the formation of the complex between HMCP and ct-DNA.

Data availability

The data that support the findings of this study are available on request from the corresponding author.

Conflicts of interest

There are no conflicts to declare.

Acknowledgements

The authors thank CSIR (No. 01(2992)/19/EMR-II) and SERB (No. EEQ/2018/000266), New Delhi, India for financial support.

Notes and references

1 R. Emas, The Concept of Sustainable Development: Definition and Defining Principles, in *Brief for GSDR*, Florida International University, 2015, pp. 1–3.
2 A. Frio, R. Janeiro, S. M. Viana, C. S. Valladares and B. P. Duarte, *Rev. Bras. Geocienc.*, 2001, 6.
3 K. Brodowska and E. Łodyga-Chruscińska, *Chemik*, 2014, **68**, 129–134.
4 S. Kumar, D. N. Dhar and P. N. Saxena, *J. Sci. Ind. Res.*, 2009, **68**, 181–187.
5 A. M. Abu-Dief and I. M. A. Mohamed, *J. Basic Appl. Sci.*, 2015, **4**, 119–133.

6 P. G. Cozzi, *Chem. Soc. Rev.*, 2004, **33**, 410–421.
7 D. T. Quang and J. S. Kim, *Chem. Rev.*, 2010, **110**, 6280–6301.
8 F. J. Hayes, H. B. Halsall and W. R. Heineman, *Anal. Chem.*, 1994, **66**, 1860–1865.
9 B. Valeur and I. Leray, *Coord. Chem. Rev.*, 2000, **205**, 3–40.
10 L. Prodi, F. Bolletta, M. Montalti and N. Zaccheroni, *Chem. Rev.*, 2000, **205**, 59–83.
11 G. C. Woodson, *Bone*, 1998, **22**, 695–698.
12 C. S. Cronan, W. J. Walker and P. R. Bloom, *Nature*, 1986, **324**, 140–143.
13 T. P. Flaten, *Brain Res. Bull.*, 2001, **55**, 187–196.
14 G. Berthon, *Coord. Chem. Rev.*, 1996, **149**, 241–280.
15 M. G. Soni, S. M. White, W. G. Flamm and G. A. Burdock, *Regul. Toxicol. Pharmacol.*, 2001, **33**, 66–79.
16 E. Gauthier, I. Fortier, F. Courchesne, P. Pepin, J. Mortimer and D. Gauvreau, *Environ. Res.*, 2000, **84**, 234–246.
17 G. D. Fasman, *Coord. Chem. Rev.*, 1996, **149**, 125–165.
18 D. Krewski, R. A. Yokel, E. Nieboer, D. Borchelt, J. Cohen, S. Kacew, J. Lindsay, A. M. Mahfouz and V. Rondeau, *J. Toxicol. Environ. Health, Part B*, 2009, **10**, 1–269.
19 G. C. Woodson, *Bone*, 1998, **22**, 695–698.
20 J. Barcelo and C. Poschenrieder, *Environ. Exp. Bot.*, 2002, **48**, 75–92.
21 WHO, *Guidelines for Drinking-Water Quality*, World Health Organization, 4th edn, 2017.
22 T. P. Flaten, *Brain Res. Bull.*, 2001, **55**, 187–196.
23 G. Berthon, *Coord. Chem. Rev.*, 1996, **149**, 241–280.
24 M. G. Soni, S. M. White, W. G. Flamm and G. A. Burdock, *Regul. Toxicol. Pharmacol.*, 2001, **33**, 66–79.
25 E. Gauthier, I. Fortier, F. Courchesne, P. Pepin, J. Mortimer and D. Gauvreau, *Environ. Res.*, 2000, **84**, 234–246.
26 G. D. Fasman, *Coord. Chem. Rev.*, 1996, **149**, 125–165.
27 D. Krewski, R. A. Yokel, E. Nieboer, D. Borchelt, J. Cohen, S. Kacew, J. Lindsay, A. M. Mahfouz and V. Rondeau, *J. Toxicol. Environ. Health, Part B*, 2009, **10**, 1–269.
28 B. Das, M. Dolai, A. Ghosh, A. Dhara, A. Das Mahapatra, D. Chattopadhyay, S. Mabhai, A. Jana, S. Dey and A. Misra, *Anal. Methods*, 2021, **13**, 4266.
29 C. V. Kumar and E. H. Asuncion, *J. Am. Chem. Soc.*, 1993, **115**, 8547–8553.
30 X. Chen, L. Zhang, K. Zhou, E. Davies, K. Sugden, I. Bennion, M. Hughes and A. Hine, *Opt. Lett.*, 2007, **32**, 2541–2543.
31 W. A. Durai and A. Ramu, *ChemistrySelect*, 2020, **5**, 4778–4785.
32 S. K. Sheeta, B. Sena, R. Thounaojamb, K. Aguanb and S. Khatua, *J. Photochem. Photobiol., A*, 2017, **332**, 101–111.
33 A. P. de Silva, *Molecular Logic-Based Computation*, Royal Society of Chemistry, Cambridge, UK, 2012.
34 S. Erbas-Cakmak, S. Kolemen, A. C. Sedgwick, T. Gunnlaugsson, T. D. James, J. Yoon and E. U. Akkaya, *Chem. Soc. Rev.*, 2018, **47**, 2228–2248.
35 J. Andreasson and U. Pischel, *Chem. Soc. Rev.*, 2018, **47**, 2266–2279.
36 B. Das, S. Dey, G. P. Maiti, A. Bhattacharjee, A. Dhara and A. Jana, *New J. Chem.*, 2018, **42**, 9424–9435.
37 S. L. Hu, J. J. Song, G. Y. Wu, C. X. Cheng and Q. Gao, *Spectrochim. Acta, Part A*, 2015, **136**, 1188–1194.
38 S. Zhang, Y. Wang and H. Xu, *Spectrochim. Acta, Part A*, 2022, **275**, 121193.
39 J. Wang, L. Feng, J. Chao, Y. Wang and S. Shuang, *Anal. Methods*, 2019, **11**, 5598.
40 I. H. Hwang, Y. W. Choi, K. B. Kim, G. J. Park, J. J. Lee, L. Nguyen, I. Noh and C. Kim, *New J. Chem.*, 2016, **40**, 171–178.
41 A. Das and G. Das, *New J. Chem.*, 2022, **46**, 19002–19008.
42 C. Liu, L. Liu, T. Li, K. Liu and Z. Yang, *Inorg. Chim. Acta*, 2020, **502**, 119327.
43 N. Behera and V. Manivannan, *J. Photochem. Photobiol., A*, 2018, **353**, 77–85.
44 A. Maji, R. Naskar, D. Mitra, S. Gharami, N. Murmu and T. K. Mondal, *J. Fluoresc.*, 2023, **33**, 2403–2414.
45 J. Wang, L. Feng, J. Chao, Y. Wang and S. Shuang, *Anal. Methods*, 2019, **11**, 5598.
46 S. Gharami, K. Aich, D. Sarkar, P. Ghosh, N. Murmu and T. K. Mondal, *New J. Chem.*, 2019, **43**, 1857–1863.
47 S. OğuzTümay, A. Şenocak and A. Mermer, *New J. Chem.*, 2021, **45**, 18400–18411.
48 A. Maji, A. Biswas, B. Bera and T. K. Mondal, *Anal. Methods*, 2023, **15**, 6417–6424.
49 U. Saha, B. Das, M. Dolai, J. Butcher and G. Suresh Kumar, *ACS Omega*, 2020, **5**(29), 18411–18423.
50 S. O. Tümay, A. Şenocak and A. Mermer, *New J. Chem.*, 2021, **45**, 18400–18411.
51 A. Saravanan, S. Shyamsivappan, N. K. Kalagatur, T. Suresh, N. Maroli, N. Bhuvanesh, P. Kolandaivel and P. S. Mohan, *Spectrochim. Acta, Part A*, 2020, **241**, 118684.
52 S. Gharami, K. Aich, D. Sarkar, P. Ghosh, N. Murmu and T. K. Mondal, *New J. Chem.*, 2019, **43**, 1857–1863.
53 A. D. Becke, *J. Chem. Phys.*, 1993, **98**, 5648–5652.
54 M. J. Frisch, G. W. Trucks, H. B. Schlegel, G. E. Scuseria, M. A. Robb, J. R. Cheeseman, G. Scalmani, V. Barone, B. Mennucci, G. A. Petersson, H. Nakatsuji, M. Caricato, X. Li, H. P. Hratchian, A. F. Izmaylov, J. Bloino, G. Zheng, J. L. Sonnenberg, M. Hada, M. Ehara, K. Toyota, R. Fukuda, J. Hasegawa, M. Ishida, T. Nakajima, Y. Honda, O. Kitao, H. Nakai, T. Vreven, J. A. Montgomery, Jr., J. E. Peralta, F. Ogliaro, M. Bearpark, J. J. Heyd, E. Brothers, K. N. Kudin, V. N. Staroverov, R. Kobayashi, J. Normand, K. Raghavachari, A. Rendell, J. C. Burant, S. S. Iyengar, J. Tomasi, M. Cossi, N. Rega, J. M. Millam, M. Klene, J. E. Knox, J. B. Cross, V. Bakken, C. Adamo, J. Jaramillo, R. Gomperts, R. E. Stratmann, O. Yazyev, A. J. Austin, R. Cammi, C. Pomelli, J. W. Ochterski, R. L. Martin, K. Morokuma, V. G. Zakrzewski, G. A. Voth, P. Salvador, J. J. Dannenberg, S. Dapprich, A. D. Daniels, Ö. Farkas, J. B. Foresman, J. V. Ortiz, J. Cioslowski and D. J. Fox, *Gaussian 09, Revision D.01*, Gaussian, Inc., Wallingford CT, 2009.
55 F. Furche and R. Ahlrichs, *J. Chem. Phys.*, 2002, **117**, 7433.
56 R. Bauernschmitt and R. Ahlrichs, *Chem. Phys. Lett.*, 1996, **256**, 454–464.

57 R. E. Stratmann, G. E. Scuseria and M. J. Frisch, *J. Chem. Phys.*, 1998, **109**, 8218–8224.

58 M. E. Casida, C. Jamorski, K. C. Casida and D. R. Salahub, *J. Chem. Phys.*, 1998, **108**, 4439–4449.